Confining Spirocyclic Fluorescein in an Asymmetric Solid-State Nanochannel: A Simple and Versatile Design Concept for Fabricating Integrated Nanofluidic Diodes with Adjustable Surface Chemistry

*Qi Zhao, Hai-Long Qian, Zhu-Ying Yan, Xu-Qin Ran, and Xiu-Ping Yan**

Using small molecules to integrate multifunctional surfaces within a nanopore is an effective way to endow smart responsibilities of nanofluidic diodes. However, the complex synthesis of the small molecules hinders their further application in achieving multifunctional surfaces. Here, a simple and versatile design concept is reported for fabricating bioinspired integrated nanofluidic diodes with adjustable surface chemistry by confining a spirocyclic fluorescein derivative, 6-aminofluorescein (6-AF), within an asymmetric track-etched nanopore. The pH-dependent open-close of lactone ring in 6-AF allows facile fabrication of a pH-gated nanofluidic diode, confirmed with finite element simulations. This pH-gated nanofluidic diode also shows high specificity for sensing 3-nitropropionic acid (3-NPA), indicating its potential applications in food safety. Moreover, three functional nanofluidic diodes are successfully constructed via a regioselective Vilsmeier reaction between 6-AF and N-methylformanilide, the electrophilic addition reaction between 6-AF and propargyl bromide, and a highly controllable reduction process between 6-AF and $NaBH_4/I_2$. The combination of asymmetric nanopores with small molecules not only expands traditional fluorescent spirocyclic molecules to the realm of electrochemistry but also offers valuable insights for the achievement of novel fluorescence-electrochemical coupling detection methods. Besides, the introduction of spirocyclic small molecules to asymmetric nanopores serves as an inspiration source to explore new design concepts for nanofluidic devices.

1. Introduction

Living organisms employ asymmetric ion channels to regulate the transportation of diverse ions across cellular membranes, which plays pivotal roles in virtually all fundamental physiological processes.[1–4] However, it is challenging to isolate these protein ion channels from the phospholipid bilayer membrane for potential applications due to their fragility and instability. The utilization of asymmetric solid-state nanochannel membranes to fabricate bioinspired nanofluidic diodes is a wise choice because it can not only overcome the fragility of phospholipid membranes but also mimic the ion selectivity and ion rectifying properties of the biological ion channels.[5,6] These interesting ionic properties of the bioinspired nanofluidic diodes are attributed to the fine regulation of surface chemistry in the nanoconfined spaces. Based on this, diverse bioinspired nanofluidic devices have been developed to respond to external stimuli.[7–13] The key point of the solid-state nanochannels focuses on triggering changes in the surface charge or wettability of the inner pore walls after external stimulus, which ultimately changes the species and concentration of ions inside the nanopore. Therefore, it is of paramount importance to develop novel approaches for manipulating the surface chemistry of asymmetric nanopores in order to exert precise control over the ion transport performance of nanofluidic devices and subsequently apply them in practical scenarios.

Chemical grafting offers significant advantages in terms of selectivity and stability compared to the non-covalent modifications and emerges as a wide approach for precisely adjusting the surface chemistry of bioinspired nanofluidic diodes.[14–19] To date, diverse functional surfaces have been successfully fabricated by grafting responsive factors, such as small molecules,[20] aptamer,[21] DNA,[22] polymer,[23,24] metal–organic frameworks,[25] covalent-organic frameworks,[26] and hydrogels,[27] onto the inner surface of asymmetric solid-state nanochannels. Despite these significant achievements, all

Q. Zhao, H.-L. Qian, X.-Q. Ran, X.-P. Yan
Institute of Analytical Food Safety
School of Food Science and Technology
Jiangnan University
Wuxi 214122, China
E-mail: xpyan@jiangnan.edu.cn
Z.-Y. Yan, X.-P. Yan
Analysis and Testing Center
Jiangnan University
Wuxi 214122, China
X.-P. Yan
Key Laboratory of Synthetic and Biological Colloids
Ministry of Education
Jiangnan University
Wuxi 214122, China

The ORCID identification number(s) for the author(s) of this article can be found under https://doi.org/10.1002/smll.202501424

DOI: 10.1002/smll.202501424

surfaces consistently exhibit a singular function. Especially for small molecules, the molecular structure of these response factors should be tailored to accommodate diverse properties in order to fulfill the desired functional surface. This undoubtedly poses a challenge to the synthesis because not only the molecular structure should be adjusted to a specific stimulus, but also the designed molecule should be effectively connected to the inner surface of the nanochannel. Therefore, it is highly significant to integrate multiple functionalities within a nanopore to mitigate the challenges associated with molecular synthesis.

Extensive utilization of fluorescein and rhodamine provides a viable approach to achieve integrated functional surfaces. Fluorescein and rhodamine, two classical fluorescent dyes, have gained significant attention since their discovery in the 19th century.[28] A large variety of research has been conducted to elucidate the relationship between molecular structure and functional properties of these dyes. In this context, one intriguing aspect is their capability of spirocyclization.[29–37] There is a dynamic equilibrium between a lipophilic, spirocyclic form (ring-closed) and the polar, ionic (ring-opened) forms in these dyes, which results in modification to the fixed charge and wettability characteristics. Moreover, the presence of a lactone ring, phenol groups, as well as amino groups in these small molecules create favorable conditions for further modification and functionalization. Consequently, confining these fluorescent dye molecules within asymmetric solid-state nanochannels not only offers a crucial approach for fabricating functional nanofluidic diodes but also helps to expand the application range of these dye molecules, injecting renewed vitality into age-old studies. Even so, previous research primarily focused on the development of nanofluidic diodes with specific functionalities.[38,39] The utilization of these small molecules as fundamental units to build multifunctional nanofluidic devices is highly appealing.

Herein, we present a novel and versatile approach for fabricating nanofluidic diodes with diverse functional characteristics by confining fluorescent dye molecules within asymmetric solid-state nanochannels. A pH-responsive nanofluidic diode was fabricated by exploring the change of the surface chemistry inside the 6-aminofluorescein (6-AF) modified conical nanochannels. In this nanosized system, the 6-AF molecules exhibited distinct fixed charge and polarity in response to variations in pH due to the dynamic equilibrium between a lipophilic, spirocyclic form (ring-closed) and the polar, ionic (ring-opened) forms. This nanofluidic diode also showed enhanced ion rectifying properties as compared to the unmodified asymmetric nanochannel. In addition, the 6-AF layer in the nanopore provided opportunities to manipulate the surface chemical properties of nanofluidic diodes via further modification. Aldehyde groups were introduced into the nanofluidic diode with a regioselective Vilsmeier reaction between the 6-AF layer and N-methylformanilide. Additionally, a functionalized nanofluidic diode bearing alkynyl groups was further fabricated by the electrophilic addition reaction. Moreover, dihydrofluorescein alcohols were introduced to the nanofluidic diode through a mild $NaBH_4/I_2$ strategy to easily reduce the 6-AF molecule to dihydrofluorescein alcohols. This work provides a simple and versatile design concept for fabricating integrated nanofluidic diodes with adjustable surface chemistry for potential applications in neuromodulation devices, energy conversion, and sensors.

2. Results and Discussion

The modification of 6-Aminofluoresein (6-AF) molecules on the inner surface of the polyethylene terephthalate (PET) conical nanochannel is illustrated in **Figure 1**. First, the nanochannel was asymmetrically and chemically etched in a PET foil (Figure S1a, Supporting Information). Scanning electron microscopy revealed that the diameter of the large opening of the fabricated conical nanochannel was ≈700 nm (Figure S2, Supporting Information), while the small opening is calculated to be ≈23 nm according to Equation (S1) (Supporting Information). The carboxyl groups of the etched conical nanochannel were then used to immobilize 6-AF molecules via a one-step coupling reaction (Figure 1a). A new N 1s signal in the X-ray photoelectron spectra (XPS) of the modified nanochannel indicates the successful incorporation of 6-AF molecules onto the inner surface of the conical PET nanochannels (Figure 1b; Tables S1 and S2, Supporting Information).

Current–voltage (*I*–*V*) curves were then used to verify the successful attachment of 6-AF. The largest ion rectification was shown in 0.1 M KCl solution (Figure S3, Supporting Information). It is well known that the ionic current through the nanochannels is closely related to the channel surface charge. Calculation from electroosmotic flow (EOF) data indicates that the negative surface charge density on the inner surface increased from $-0.150\ e^{-}\ nm^{-2}$ for the unmodified channel to $-0.171\ e^{-}\ nm^{-2}$ after the modification of 6-AF (Equations S2–S8, Figures S4–S7, and Table S3, Supporting Information). As the surface negative charge increased, more counterions in electrolyte solution were attracted to the inner surface pore walls and the ion current increased subsequently. As such, a considerable increase in the conductance of the conical PET nanochannel was observed after the 6-AF modification owing to the deprotonation of the 6-AF molecules at a neutral pH (Figure 1c). The modification of 6-AF molecules on the inner surface of a PET nanochannel was tracked by laser-scanning confocal microscopy (LSCM). An obvious fluorescence signal in the 6-AF-modified channel was observed (Figure 1d). Therefore, all the above results confirmed the successful construction of a biomimetic nanofluidic diode.

The effect of pH on the *I*–*V* transmission performance of the biomimetic nanofluidic diode was then explored in 0.1 M KCl solution at three typical pH values (2, 4, and 9). It is well known that fluorescein possesses ampholytic or zwitterionic properties due to the protonation and deprotonation of intramolecular spironolactone.[40] The introduction of fluorescein derivatives, 6-AF, undoubtedly provides a convenient strategy for modulating the surface charge on the inner walls of nanochannels under varying pH conditions (**Figure 2**a, bottom), owing to the various acid-base equilibriums of 6-AF molecules (Figure 2a, top). Thus, the ion transport properties of the biomimetic nanofluidic diode can be well adjusted by simply changing the pH of the KCl electrolyte solution.

Under acidic conditions (pH 2), the ionic currents for $V < 0$ were smaller than those for $V > 0$ (Figure 2b), indicating an anion selectivity and a positive rectification of the biomimetic nanofluidic diode since the protonation of the intramolecular spironolactone in the 6-AF and the secondary amine units. In contrast, as pH shifted to 9, anion forms of the 6-AF became more prevalent since the deprotonation of the intramolecular

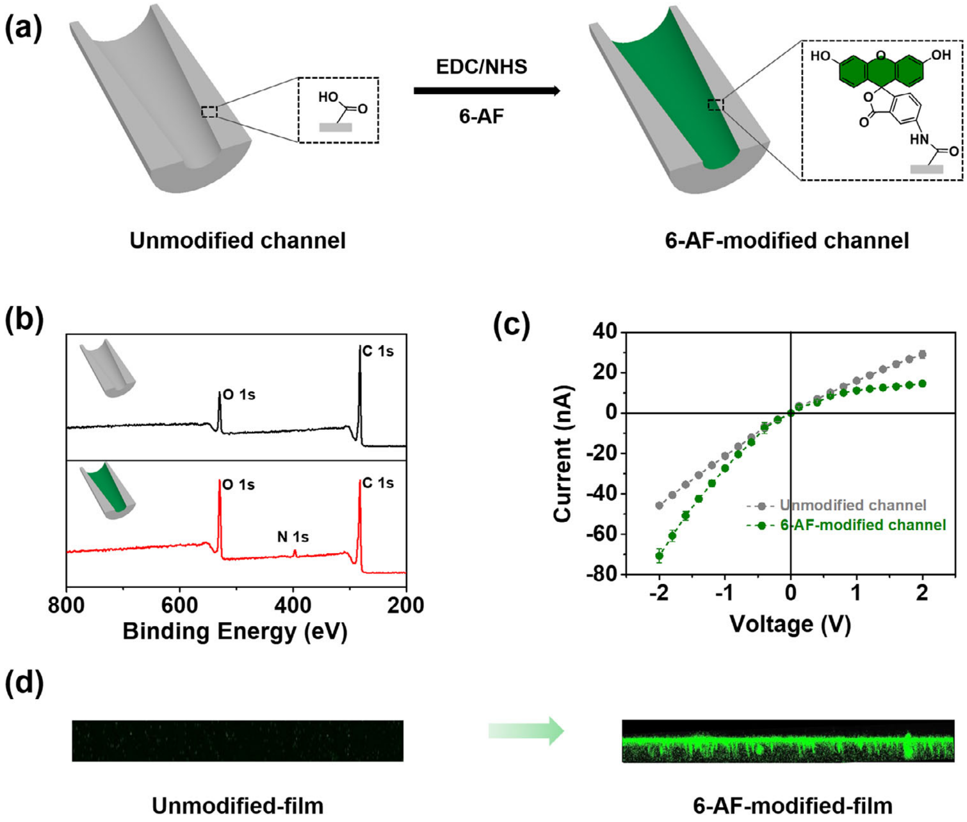

Figure 1. a) Illustration for the nanochannel modification with 6-AF molecules via a one-step coupling reaction. b) X-ray photoelectron spectra (XPS) of unmodified PET (black line) and 6-AF-modified (red line). c) Current–voltage (*I*-*V*) curves of the nanochannel before and after modification (0.1 M KCl, pH 7). d) Laser scanning confocal microscopy (LSCM) observation of the fluorescent signals before and after 6-AF modification. Error bars represent standard deviations obtained from three replicate ionic current measurements.

spironolactone, eventually making the biomimetic nanofluidic diode cation-selective, and negative-rectifiable. In this case, the ionic currents for $V < 0$ were higher than those for $V > 0$ (Figure 2d). More interestingly, the *I*–*V* curves for pH 2 and 9 were almost perfectly antisymmetric. The *I*-*V* curves showed a linear relationship at pH 4, owing to the neutral form of 6-AF molecules (Figure 2c).

We further investigated the pH-responsive behaviors of the biomimetic nanofluidic diode by comparing the characteristics of *I*–*V* curve, ionic selectivity, and ion rectifying in 0.1 M KCl with pH from 2 to 9. A rectification factor (f_{rec}) is defined (Equation S9, Supporting Information) corresponding to a positive f_{rec} to positive surface charge and a negative f_{rec} to negative surface charge. The *I*-*V* curves of the unmodified nanochannel showed weak pH-gating behavior with ion rectification direction in the negative mode from pH 2 to 9, and the absolute values of f_{rec} between 1 and 1.6 across all pH (Figure S8, Supporting Information). However, our 6-AF-modified nanochannel exhibited a significant transition in the *I*–*V* curves from the positive model to the negative model as pH increased (**Figure** 3a), indicating an alternation in ion selectivity and rectification direction. The alkaline condition gave higher f_{rec} than the acidic condition (Figure 3b), showing a greater charge density on the inner surface of the 6-AF-modified nanochannel in the alkaline environment. Therefore, confining 6-AF in an asymmetric nanopore via a chemical grafting method conferred the biomimetic nanofluidic diode with pH-gating behavior.

The net surface charge of 6-AF within nanopores often exhibits significant disparities compared to its behavior in free solution. As shown in Figure 3b, there was a transition between positive and negative rectification regimes, named non-rectifying state, in which the f_{rec} equaled to 1. This transition was observed in a pH region of 4.0–4.6 corresponding to the absence of net surface charge (Figure 3b), named the “isoelectric” region. The “isoelectric” region of fluorescein in our nanopore system is not only much narrower than that in free solution (2.1–4.3),[41] but also significantly shifted to higher pH. This observation could be attributed to charge regulation within nanopores. It was reported that the degree of charge in the confined dopamine system largely depended on the charge regulation in the nanoconfined pores.[17] The acid-base equilibrium within solid-state nanopores tended to shift to a less charged configuration to mitigate electrostatic repulsion and the system energy. Therefore, the change of the isoelectric region in our system resulted from charge regulation in the nanoconfined pores, in which the negatively charged form of 6-AF tended to exist at higher pH.

The *I*-*V* curves of the 6-AF modified nanochannel under three typical pH conditions were theoretically confirmed. A finite element computation proceeded based on the Poisson and Nernst–Planck (PNP) equations (Equations S10–S14 and Figure S9,

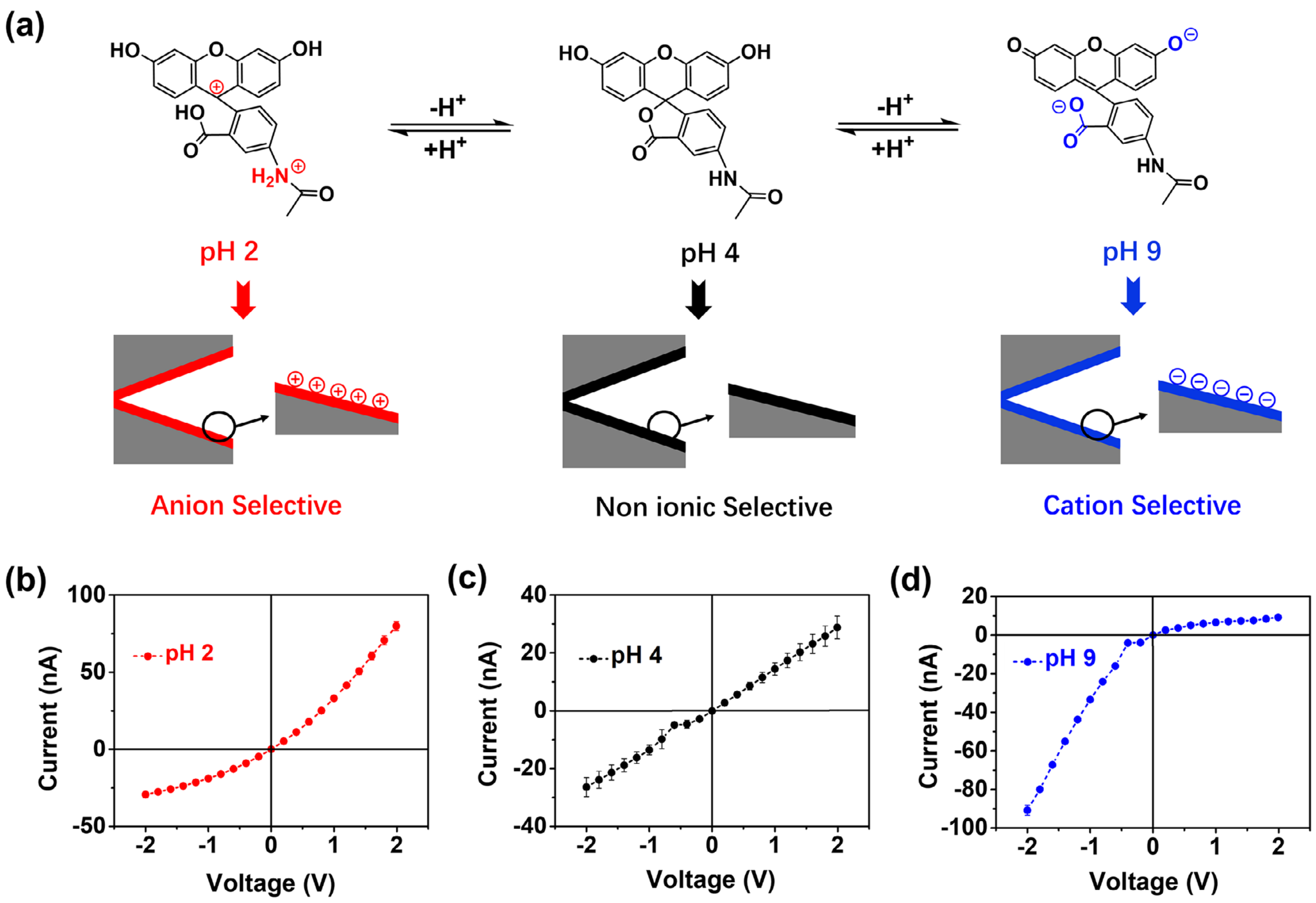

Figure 2. a) Different protonation states of 6-AF molecules and the resulting surface charges at different pH values. *I-V* curves of the 6-AF-modified nanochannel under different pH conditions: b) pH 2; c) pH 4; and d) pH 9. Error bars represent standard deviations obtained from three ionic current measurements.

Supporting Information). The charge densities of the 6-AF-modified nanochannel for pH 2, 4, and 9 were set at −0.4, 0, and 0.4 e nm^{-2}, respectively. The obtained theoretical *I-V* curves were in good agreement with experimental results (**Figure** 4b *cf.* 4a). As shown in Figure 4b, the *I-V* curve at pH 2 demonstrated a positive rectification, while the rectifying state turned to the negative state at pH 9. In addition, there was a linear relationship at pH 4 in the *I-V* curve. Therefore, the consistency between the experimental and theoretical results strongly confirmed the feasibility of constructing a biomimetic nanofluidic diode with pH-gating behaviors by confining 6-AF in an asymmetric nanopore.

The 6-AF-modified nanofluidic diode underwent cyclic treatment with 0.1 м KCl electrolyte solution at pH 2 and 11 for

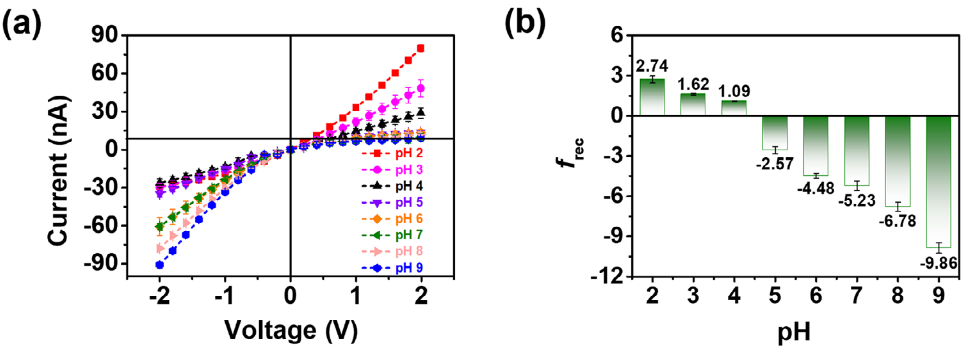

Figure 3. a) *I-V* curves of the 6-AF-modified nanochannel under different pH conditions. b) Rectification rate (f_{rec}) as a function of pH. Error bars represent standard deviations obtained from three ionic current measurements.

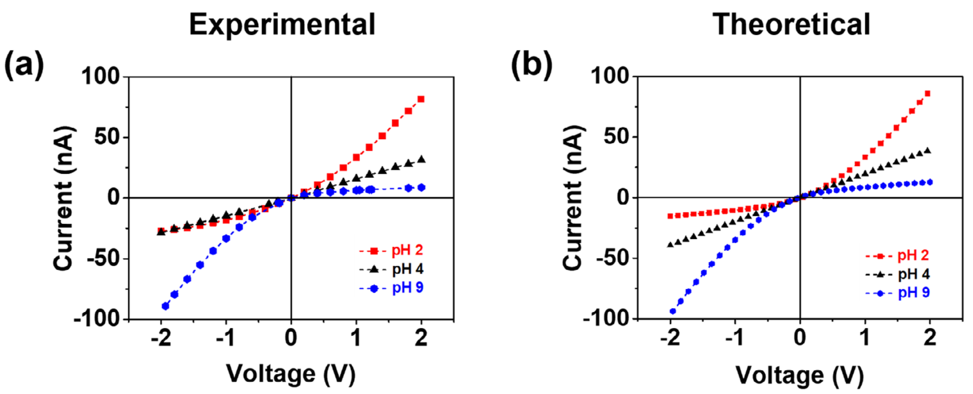

Figure 4. *I–V* curves of the amphoteric nanofluidic diode at pH 2, 4, and 9. a) Experimental results. b) Theoretical results from a finite-element computation. The fitting procedure gave an uncertainty range of 10% for the estimated surface charge density.

five cycles to study its reversibility and stability. The *I–V* curves of the nanofluidic diode showed a reversible switchability at the five cyclic experiments (Figure S10a,b, Supporting Information). In addition, the 6-AF-modified nanofluidic diode also exhibited excellent stability due to its mechanism of covalent interaction. The stability test was estimated by a 240-min examination (Figure S11, Supporting Information). The ionic rectification was stable and lasted at least 240 min, indicating excellent stability of the 6-AF-modified nanofluidic diode. The above results show the excellent reversibility and stability of the 6-AF-modified nanofluidic diode.

The developed 6-AF-modified nanofluidic diode was further investigated for sensing 3-nitropropionic acid (3-NPA), a toxic mycotoxin in moldy sugarcane that represents a significant category of neurotoxins.[42,43] Here, for the first time, the 6-AF-modified nanofluidic diode was used as an electrochemical sensor for the detection of 3-NPA. The determination of 3-NPA was performed on a laboratory-built nanochannel system (Figure S12, Supporting Information). The effect of pH on the performance of the 6-AF-modified nanofluidic diodes for 3-NPA sensing was explored first. The test was performed in 0.1 м KCl at four different pH conditions (2, 4, 7, and 9) (**Figure 5**). At pH 2, the addition of 3-NPA (0.1 mм) to the 6-AF-modified nanofluidic device enhanced the positive surface charges, thus reducing the ionic current rectification by increasing the ionic current at positive potentials (Figure 5a,e).

At pH 4, the f_{rec} equaled to 1 and the surface charge of the nanochannels was effectively neutral. The presence of 3-NPA (0.1 mм) in solution was not sufficient to cause a change in the surface charge of the 6-AF-modified nanofluidic diode. Both the ionic current in both potentials and the ionic rectification remained unchanged (Figure 5b,e).

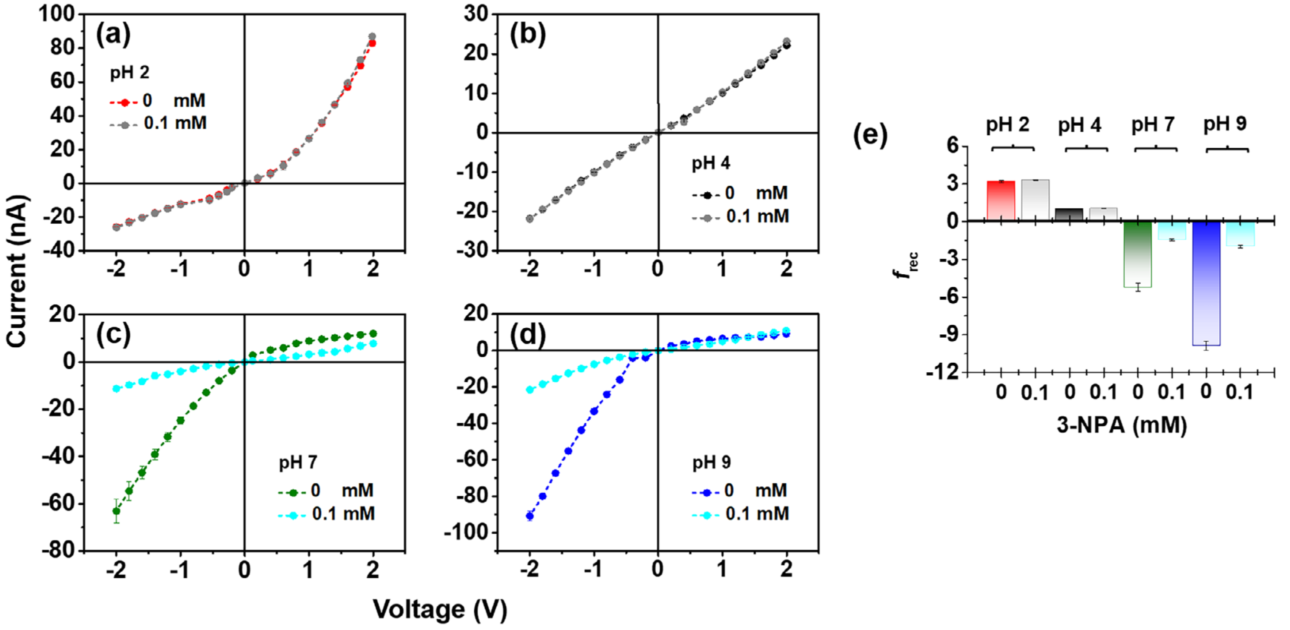

Figure 5. Current–voltage curves for the 6-AF-modified nanofluidic diode measured for each of the four regions within the pH-effective range (2–9) in the absence and presence of 3-NPA: a) acid, b) neutral, c), and d) alkaline regions. e) Rectification factors (f_{rec}) calculated for each region in the absence and presence of 3-NPA. Error bars represent standard deviations obtained from three replicate ionic current measurements.

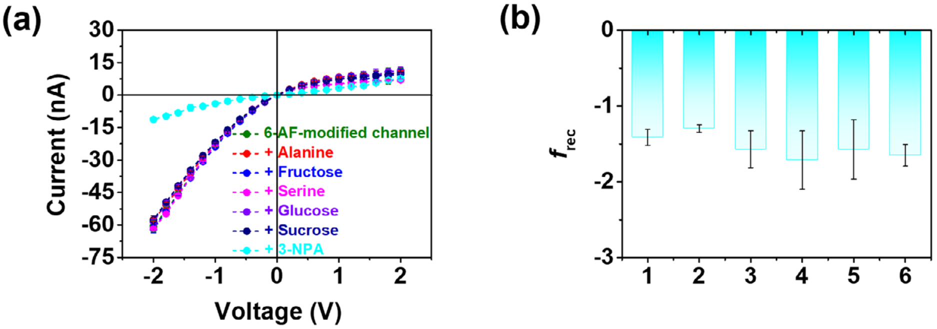

Figure 6. a) *I*--*V* curves of the 6-AF-modified nanofluidic diode after adding 0.1 mM saccharides. b) Effects of other saccharides (1 mM) on the current decrease rate of the 6-AF-modified nanofluidic diode (1, 3-NPA (0.1 mM) + alanine; 2, 3-NPA (0.1 mM) + fructose; 3, 3-NPA (0.1 mM) + serine; 4, 3-NPA (0.1 mM) + glucose; 5, 3-NPA (0.1 mM) + sucrose; 6, 3-NPA (0.1 mM) + alanine + fructose + serine + glucose + sucrose). Error bars represent standard deviations obtained from three replicate ionic current measurements.

At pH 7, adding 3-NPA (0.1 mM) to the solution led to a transition between a negatively charged state (cation-selective) to a non-charged state (nonselective) of the inner surface of the 6-AF-modified nanofluidic diode. This transition resulted in a decrease in ionic current at both negative potentials and positive potentials (Figure 5c). Meanwhile, the rectification efficiency decreased due to the reduction of the ionic selectivity of the 6-AF-modified nanofluidic diode (Figure 5e). A similar pattern of transformation was observed at pH 9 after adding 3-NPA (0.1 mM) to the solution (Figure 5d,e).

Based on the above results, we then evaluated the selectivity of 6-AF-modified nanofluidic diode for 3-NPA sensing. The tests were performed in 0.1 M KCl at pH 7. Other competitive neurotoxins including alanine, fructose, serine, glucose, and sucrose were chosen for comparison and their corresponding *I*–*V* curves were also measured. As shown in **Figure 6**a, the ionic current at -2 V as well as f_{rec} significantly decreased after the reaction of 3-NPA to the 6-AF-modified nanofluidic diode, while only slightly changed in the presence of other neurotoxins of alanine, fructose, serine, glucose, and sucrose. However, the ionic current at 2 V remained constant. Moreover, the addition of 10 times higher concentration of the saccharides than 3-NPA gave little effect on the current decrease rate of the proposed 6-AF-modified nanofluidic diode in the presence of 3-NPA (Figure 6b), indicating its high specificity for 3-NPA.

We finally explored the chemical diversity of the 6-AF layer to obtain diverse functional surfaces. Three typical reactions, a regioselective Vilomeler reaction, the electrophilic addition reaction, and a highly controllable reduction process were selected to attain the functionalized nanofluidic diodes bearing aldehyde group, alkynyl groups, and hydroxyl groups, respectively. The aldehyde groups were introduced into the nanofluidic diode with a regioselective Vilomeler reaction between the 6-AF layer and N-methylformanide,[44] named 6-AF-CHO-modified nanochannel. Meanwhile, a functionalized nanofluidic diode bearing alkynyl groups, 6-AF-C≡C-modified nanochannel, was fabricated via the electrophilic addition reaction between the 6-AF molecule and propargyl bromide. In addition, a 6-AF-OH-modified nanochannel was obtained via a mild $NaBH_4/I_2$ strategy to easily reduce the 6-AF molecule to dihydrofluorescein alcohols (**Figure 7**a). The successful modification was confirmed by XPS, contact angle measurements, and ion current experiments. New characteristic peaks of C 1s for C_6H_5CHO appeared after modification (Figure 7b), indicating the successful attachment of aldehyde groups in the 6-AF layer. The appearance of new characteristic peaks of C 1s for C≡C and the disappearance of O 1s for OH after the modification shows the successful construction of the 6-AF-C≡C nanochannel. In addition, the disappearance of C 1s for O—C=O after the modification demonstrates the successful fabrication of 6-AF-OH-modified nanochannel (Figure 7b,c; Tables S4–S6, Supporting Information). Finally, the *I*–*V* curves of 6-AF-modified nanochannels after the modification were obtained in an electrolyte solution of 0.1 M KCl at pH 7. The introduction of aldehyde groups into the 6-AF layer of the nanochannel led to a significant decrease in the current and ionic rectification ratio due to the decrease in surface wettability (Figure 7d,e). The attachment of alkynyl groups via the electrophilic addition reaction exhibited the same trend in current and rectification due to the decrease of surface wettability, as compared to the 6-AF-CHO-modified nanochannel (Figure 7d,e). On the contrary, the 6-AF-OH-modified nanochannel showed an increase in the current and ionic rectification ratio due to the enhancement in the surface wettability (Figure 7d,e). Therefore, diverse high-performance nanofluidic diodes can be fabricated with 6-AF as building blocks in combination with regioselective Vilomeler reaction and the electrophilic addition reaction, or other reactions based on the spirocyclization of 6-AF molecules.

3. Conclusion

We have developed a bioinspired integrated nanofluidic diode with adjustable surface chemical properties by confining a fluorescein derivative, 6-aminofluorescein (6-AF), a small fluorescent molecule, within an asymmetric solid-state nanochannel via a one-step coupling reaction. The confinement of 6-AF in an asymmetric nanochannel enables precise control of the charge and polarity on the inner surface of the nanofluidic diode to regulate the ionic transport performance of the nanofluidic device. The pH-dependent open-close of the lactone ring in 6-AF allows the construction of a pH-gating nanofluidic diode, confirmed with finite element simulations. Furthermore, confining 6-AF within an asymmetric nanochannel facilitates the generation of diverse high-performance nanofluidic diodes without complex synthesis. In addition, 6-AF can be used as building blocks for facile

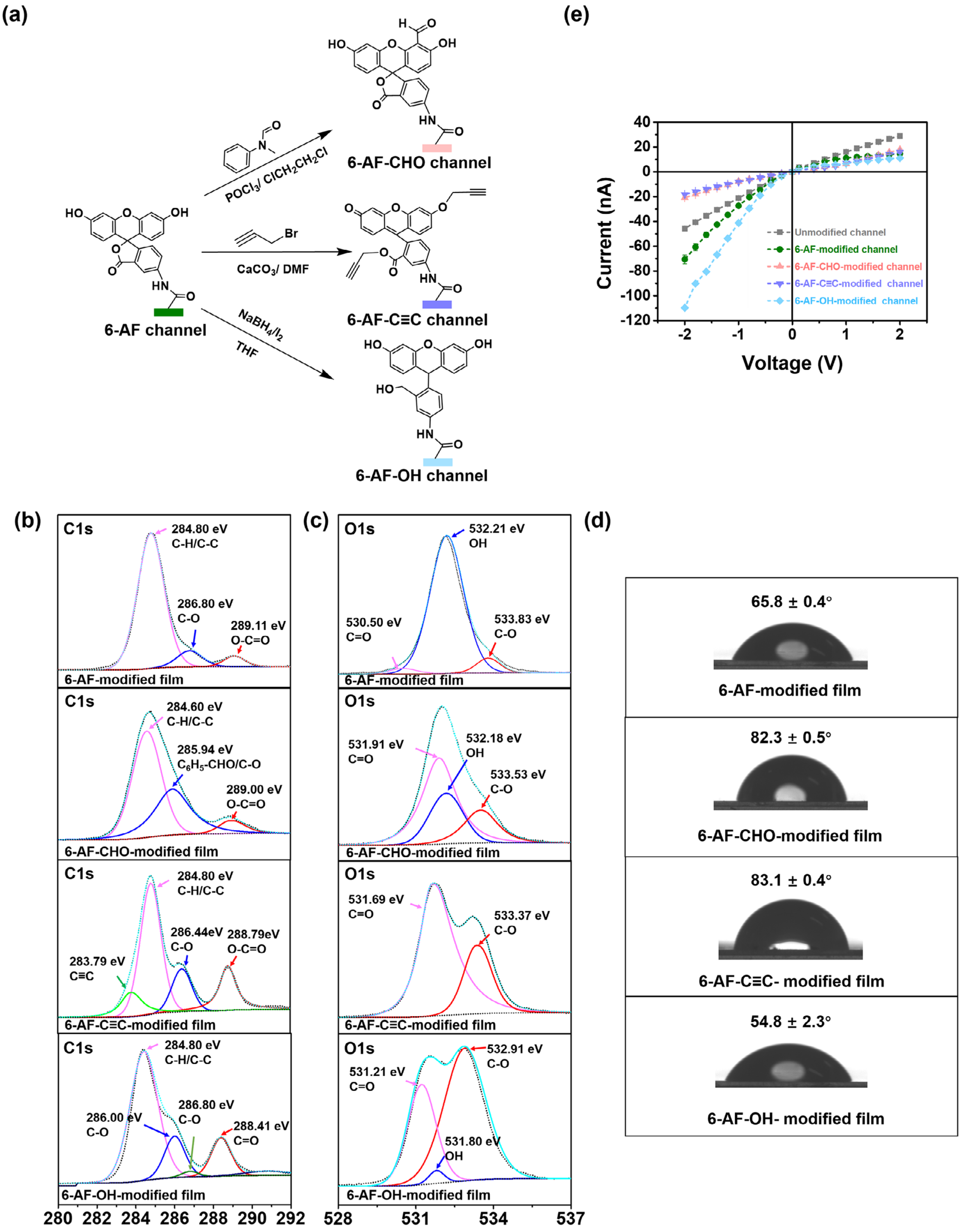

Figure 7. a) Illustration for the functionalization of 6-AF-modified nanochannel. Deconvolution analysis of the XPS spectra of 6-AF-film, 6-AF-CHO film, and 6-AF-C≡C film (dashed lines: raw curves, cyan lines: fitting curves): b) C 1s; c) O 1s. d) Contact angle measurement of 6-AF-film, 6-AF-CHO film, and 6-AF-C≡C film. e) *I–V* curves of the 6-AF-modified nanochannel before and after 6-AF-CHO functionalization and 6-AF-C≡C modification.

further necessary modification due to a rich array of functional groups such as hydroxyl and lactone rings in 6-AF. As such, we have successfully fabricated a nanofluidic diode-bearing aldehyde group in the 6-AF layers via a regioselective Vilsmeier reaction between 6-AF and *N*-methylformanilide, an alkynyl group functional nanofluidic diode based on the electrophilic addition reaction between 6-AF and propargyl bromide, and a hydroxyl group functional nanofluidic diode through a highly controllable reduction process. The combination of asymmetric nanopores with small molecules not only expands traditional fluorescent small molecules with lactone rings to the realm of electrochemistry but also offers valuable insights for the achievement of novel fluorescence-electrochemical coupling detection methods. More importantly, the introduction of fluorescent small molecules to asymmetric nanopores serves as an inspiration source to explore new design concepts for nanofluidic devices.

Supporting Information

Supporting Information is available from the Wiley Online Library or from the author.

Acknowledgements

This work was supported by the National Natural Science Foundation of China (No. 42421005 and 22176073).

Conflict of Interest

The authors declare no conflict of interest.

Data Availability Statement

The data that support the findings of this study are available in the supplementary material of this article.

Keywords

asymmetric solid-state nanochannels, electrochemistry, fluorescein, nanofluidic diodes, surface chemistry

Received: February 4, 2025
Published online:

---

[1] D. A. Doyle, J. M. Cabral, R. A. Pfuetzner, A. Kuo, J. M. Gulbis, S. L. Cohen, B. T. Chait, R. MacKinnon, *Science* **1998**, *280*, 69.
[2] E. Gouaux, R. MacKinnon, *Science* **2005**, *310*, 1461.
[3] R. J. White, E. N. Ervin, T. Yang, X. Chen, S. Daniel, P. S. Cremer, H. S. White, *J. Am. Chem. Soc.* **2007**, *129*, 11766.
[4] J. Xu, D. A. Lavan, *Nat. Nanotechnol.* **2008**, *3*, 666.
[5] Z. Zhang, L. Wen, L. Jiang, *Chem. Soc. Rev.* **2018**, *47*, 322.
[6] G. Pérez-Mitta, A. G. Albesa, C. Trautmann, M. E. Toimil-Molares, O. Azzaroni, *Chem. Sci.* **2017**, *8*, 890.
[7] R. Qian, M. Wu, Z. Yang, Y. Wu, W. Guo, Z. Zhou, X. Wang, D. Li, Y. Lu, *Nat. Commun.* **2024**, *15*, 2051.
[8] W.-Q. Zhang, Y.-D. Tu, H. Liu, R. Liu, X.-J. Zhang, L. Jiang, Y. Huang, F. Xia, *Angew. Chem., Int. Ed.* **2024**, *63*, 202316434.
[9] S. Khatri, P. Pandey, G. Mejia, G. Ghimire, F. Leng, J. He, *J. Am. Chem. Soc.* **2023**, *145*, 28075.
[10] D. Zhang, Y. Sun, Z. Wang, F. Liu, X. Zhang, *Nat. Commun.* **2023**, *14*, 1901.
[11] H. Ding, K. Liu, X. Zhao, B. Su, D. Jiang, *J. Am. Chem. Soc.* **2023**, *145*, 22433.
[12] L. Zhou, R. Yang, X. Li, N. Dong, B. Zhu, J. Wang, X. Lin, B. Su, *J. Am. Chem. Soc.* **2023**, *145*, 23727.
[13] Y. Huang, H. Zeng, L. Xie, R. Gao, S. Zhou, Q. Liang, X. Zhang, K. Liang, L. Jian, B. Kong, *J. Am. Chem. Soc.* **2022**, *144*, 13794.
[14] Y. Teng, X.-Y. Kong, P. Liu, Y. Qian, Y. Hu, L. Fu, W. Xin, L. Jiang, L. Wen, *Nano Res.* **2021**, *14*, 1421.
[15] C.-Y. Lin, C. Combs, Y.-S. Su, L.-H. Yeh, Z. S. Siwy, *J. Am. Chem. Soc.* **2019**, *141*, 3691.
[16] J. Cai, W. Ma, L. Xu, C. Hao, M. Sun, X. Wu, F. M. Colombari, F. d. Moura, M. C. Silva, E. B. Carneiro-Neto, E. C. Pereira, H. Kuang, C. Xu, *Angew. Chem., Int. Ed.* **2019**, *58*, 17418.
[17] G. Pérez-Mitta, J. S. Tuninetti, W. Knoll, C. Trautmann, M. E. Toimil-Molares, O. Azzaroni, *J. Am. Chem. Soc.* **2015**, *137*, 6011.
[18] G. Pérez-Mitta, W. A. Marmisollé, C. Trautmann, M. E. Toimil-Molares, O. Azzaroni, *J. Am. Chem. Soc.* **2015**, *137*, 15382.
[19] M. Ali, B. Yameen, J. Cervera, P. Ramírez, R. Neumann, W. Ensinger, W. Knoll, O. Azzaroni, *J. Am. Chem. Soc.* **2010**, *132*, 8338.
[20] Y. Liu, Y. Qian, L. Fu, C. Zhu, X. Li, Q. Wang, H. Ling, H. Du, S. Zhou, X.-Y. Kong, L. Jiang, L. Wen, *ACS Cent. Sci.* **2024**, *10*, 469.
[21] X.-Q. Ran, H.-L. Qian, X.-P. Yan, *Anal. Chem.* **2021**, *93*, 14287.
[22] S. F. Buchsbaum, G. Nguyen, S. Howorka, Z. S. Siwy, *J. Am. Chem. Soc.* **2014**, *136*, 9902.
[23] M. Li, Y. Xiong, W. Lu, X. Wang, Y. Liu, B. Na, H. Qin, M. Tang, H. Qin, M. Ye, X. Liang, G. Qing, *J. Am. Chem. Soc.* **2020**, *142*, 16324.
[24] K. Huang, I. Szleifer, *J. Am. Chem. Soc.* **2017**, *139*, 6422.
[25] J. Hou, H. Zhang, H. Wang, A. W. Thornton, K. J. Konstas, *Mater. Chem. A* **2023**, *11*, 13223.
[26] S. Zhang, J. Zhou, H. Li, *Angew. Chem., Int. Ed.* **2022**, *61*, 202204012.
[27] Y. Wu, D. Wang, I. Willner, Y. Tian, L. Jiang, *Angew. Chem., Int. Ed.* **2018**, *57*, 7790.
[28] L. D. Lavis, *Annu. Rev. Biochem.* **2017**, *86*, 825.
[29] J. B. Grimm, A. N. Tkachuk, R. Patel, S. T. Hennigan, A. Gutu, P. Dong, V. Gandin, A. M. Osowski, K. L. Holland, Z. J. Liu, T. A. Brown, L. D. Lavis, *J. Am. Chem. Soc.* **2023**, *145*, 23000.
[30] D. Si, Q. Li, Y. Bao, J. Zhang, L. Wang, *Angew. Chem., Int. Ed.* **2023**, *62*, 202307641.
[31] N. Lardon, L. Wang, A. Tschanz, P. Hoess, M. Tran, E. D'Este, J. Ries, K. Johnsson, *J. Am. Chem. Soc.* **2021**, *143*, 14592.
[32] L. Wu, J. Liu, X. Tian, R. R. Groleau, B. Feng, Y. Yang, A. C. Sedgwick, H.-H. Han, Y. Wang, H.-M. Wang, H. Fang, S. D. Bull, H. Zhang, C. Huang, Y. Zang, J. Li, X.-P. He, P. Li, B. Tang, T. D. James, J. L. Sessler, *J. Am. Chem. Soc.* **2022**, *144*, 174.
[33] E. Daniel, E.-M. Burger, F. Grün, M. S. Verma, J. Lackner, M. Lampe, B. Bühler, J. Schokolowski, G. U. Nienhaus, A. Jäschke, M. Sunbul, *Nat. Commun.* **2023**, *14*, 3879.
[34] J. B. Grimm, T. A. Brown, A. N. Tkachuk, L. D. Lavis, *ACS Cent. Sci.* **2017**, *3*, 975.
[35] L. Wang, M. Tran, E. D'Este, J. Roberti, B. Koch, L. Xue, K. Johnsson, *Nat. Chem.* **2020**, *12*, 165.
[36] R. Zhang, J. Zhao, G. Han, Z. Liu, C. Liu, C. Zhang, B. Liu, C. Jiang, R. Liu, T. Zhao, M.-Y. Han, Z. Zhang, *J. Am. Chem. Soc.* **2016**, *138*, 3769.
[37] P. D. McQueen, S. Sagoo, H. Yao, R. A. Jockusch, *Angew. Chem., Int. Ed.* **2010**, *49*, 9193.
[38] Y.-L. Liu, S.-Y. Yu, R. An, Y. Miao, D. Jiang, D. Ye, J.-J. Xu, W.-W. Zhao, *ACS Nano* **2023**, *17*, 17468.

[39] Y. Sun, S. Chen, X. Chen, Y. Xu, S. Zhang, Q. Ouyang, G. Yang, H. Li, *Nat. Commun.* **2019**, *10*, 1323.

[40] R. Sjöback, J. Nygren, M. Kubista, *Spectrochim. Acta, Part A* **1995**, *51*, L7.

[41] F. L. Guern, V. Mussard, A. Gaucher, M. Rottman, D. Prim, *Int. J. Mol. Sci.* **2020**, *21*, 9217.

[42] W. Sui, Q. Jin, T. Shi, Y. Yu, S. L. Suib, *ACS Appl. Nano Mater.* **2024**, *7*, 13457.

[43] D. Tian, X.-J. Liu, R. Feng, J.-L. Xu, J. Xu, R.-Y. Chen, L. Huang, X.-H. Bu, *ACS Appl. Mater. Interfaces* **2018**, *10*, 5618.

[44] P. P. Deshpande, F. Tagliaferri, S. F. Victory, S. Yan, D. C. Baker, *J. Org. Chem.* **1995**, *60*, 2964.